

CrossMark
click for updatesCite this: *RSC Adv.*, 2017, 7, 9847

Synthesis, mechanism and efficient modulation of a fluorescence dye by photochromic pyrazolone with energy transfer in the crystalline state†

Yinhua Li, Jixi Guo,* Anjie Liu, Dianzeng Jia,* Xueyan Wu and Yi Chen

A dual-responsive photochromic compound, 1,3-diphenyl-4-(3-chloro-4-pyridylformyl)-5-hydroxypyrazole 4-phenylsemicarbazone (**1**) based on a pyrazolone derivative with excellent reversible photochromic reactions in the crystalline state, was successfully synthesized. The new photochromic mechanism of **1** is attributed to isomerization between the enol form and keto form with proton transfer, which was confirmed by IR, XPS, crystal structure data and theoretical calculation. In order to achieve high-contrast fluorescence switch capability, two-component composite materials (TCCM) were prepared by co-aggregating. The emission intensity of fluorophore 9,10-diphenylanthracene (DPA) can be efficiently switched by the fluorescence resonance energy transfer (FRET) between the donor DPA and acceptor coloured **1** in TCCM. The fluorescence modulation ratio is found to be 79%, which is influenced by changing the content of DPA. This novel photoswitchable TCCM may have potential application as photoswitches.

Received 8th December 2016
Accepted 11th January 2017

DOI: 10.1039/c6ra27937f

rsc.li/rsc-advances

Introduction

Due to the high contrast and selectivity of fluorescence emission, bistable photoswitchable organic molecules such as diarylethene, spiropyran, azobenzene and fulgide derivatives are accentuating potential applications in fluorescence imaging, sensors, optical data storage and molecular switches.^{1–6} The fluorescence contrast of bistable switches is one of the most significant performance parameters. Therefore, enlargement of fluorescence contrast is crucial to improve resolution and diminish the side effects destructing the digitalised signals. However, some excellent single molecular photochromic compounds demonstrate weak fluorescence or low emission contrast and quantum yields under the “common situation”. To this end, many organisations are emphatically engaged in amplifying fluorescence contrast depending on energy or electron transfer from the fluorophore to photochromic compound in composites.^{7–11} Further, fluorescence contrast can be improved to inhibit destructive reading, which is one of the primary candidates for multi-addressing sensors,¹² ultra-high resolution devices^{13–15} and non-destructive readout.^{16–18} In particular, physical doping or coupling strategies are usually implemented to manufacture composite materials. However,

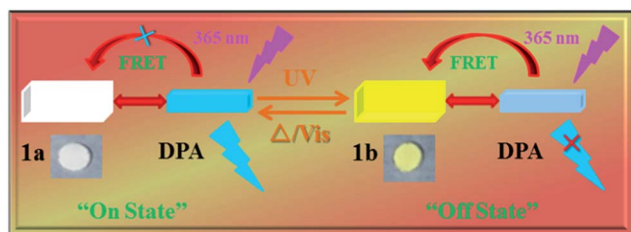
development and application of coupling methods are still restricted by intricate design and synthetic.¹⁹ Therefore, organic dyes which are doped into the photochromic system may be a good option to attain highly efficacious fluorescence switch. Intermolecular energy or electron transfer between dyes and photochromic moiety can reversibly manipulate the luminescence intensity of the fluorophore.^{20–23}

Most of the composites mentioned above are modulated in solution. However, modulation of the fluorophore luminescence in solid state is vital for practical application, which can be sensitively recognized due to its ultrahigh density and selectivity. The pyrazolone derivatives are one of the most promising candidates for application because of their photochromic conduct in the solid state. However, most of pyrazolones synthesized previously showcase irrevocable or partly reversible photochromic reactions by alternating stimulation of UV light and heating or visible light.^{24–28} In this work, a novel photochromic compound **1** with a substituted pyridine ring on the 4-position of pyrazolone ring was designed and fabricated. Photochromic compound **1** displays dual-responded reversible photochromic reactions excluding the poor fluorescent contrast in crystalline state. As we know, this is the first report on the dual-responded photochromic compound of pyrazolones. Fluorophore DPA demonstrates high fluorescent emission in crystalline state. More importantly, its emission spectra superimposed well with the absorption spectra of coloured **1**. Photochromic pyrazolone **1** might be used to modulate the fluorescence of DPA. So, TCCM were fabricated by co-aggregating the fluorophore DPA and photochromic compound **1**. The fluorescence of DPA might be efficiently controlled ON/OFF by the photochromic reactions of **1** in TCCM based on FRET (Scheme 1). To the best of our knowledge, FRET is a manifestation of

Key Laboratory of Energy Materials Chemistry, Ministry of Education, Key Laboratory of Advanced Functional Materials, Institute of Applied Chemistry, Xinjiang University, Autonomous Region, Urumqi, Xinjiang, 830046, P. R. China. E-mail: jxguo1012@163.com; jdz0991@gmail.com; Fax: +86-991-8588883; Tel: +86-991-8583083

† Electronic supplementary information (ESI) available: NMR spectra, kinetics plot of compound **1**; fluorescence decay curves, SEM; tables of crystal data, selected bond length, hydrogen bonds. CCDC 1526956. For ESI and crystallographic data in CIF or other electronic format see DOI: 10.1039/c6ra27937f





Scheme 1 Schematic diagram of fluorescence modulation for TCCM.

intermolecular energy transfer from the excitation energy of DPA to coloured **1**, which is a non-radiative energy transfer process utilising physical long-range dipole–dipole coupling.^{29,30}

Experimental section

Materials

4-Phenylsemicarbazide (PSC), 9,10-diphenylanthracene (DPA), 2-chloropyridine-4-carbonyl chloride were purchased from Aladdin Industrial Corporation. All other materials and solvents were purchased from commercial sources and special solvents were purified with standard procedures.

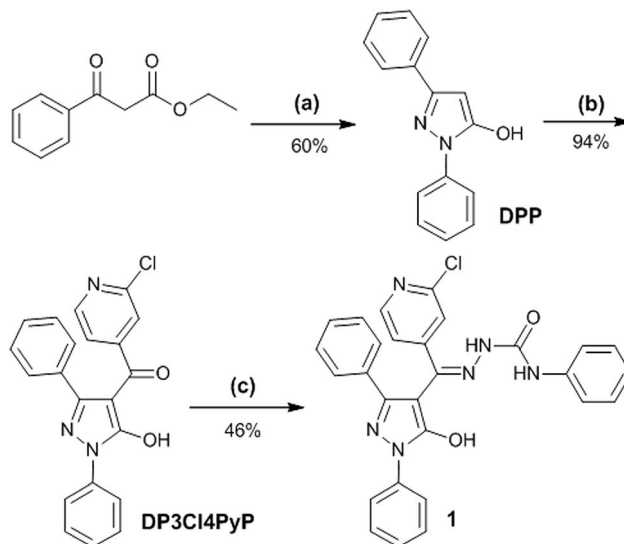
General

Melting point was recorded with a BUCHI M-560 melting point apparatus. ¹H NMR and ¹³C NMR spectra were performed on an INOVA-400 NMR spectrometer with DMSO-*d*₆ as solvent. FT-IR spectra were measured by infrared diffuse reflectance spectroscopy in the range 400–4000 cm⁻¹ on a BRUKER EQUINOX-55 spectrometer. The diffraction data were collected at 25 °C on a Bruker Smart APEX11 single crystal diffractometer equipped with a 4k CCD-detector (graphite Mo K α radiation, λ = 0.71073 Å). Absorption spectra were measured on Hitachi UV-3010 spectrometer. Fluorescence spectra were studied using a Hitachi F-4500 fluorescence spectrophotometer. Fluorescence decays were recorded on HORIBA FL-3 with 10% attenuation slices. X-Ray photoelectron spectra (XPS) were carried out using a Perkin-Elmer PHI 5300 System. Morphology and microstructure of samples were investigated by FESEM (Hitachi S-4800). X-ray powder diffraction (XRD) patterns were obtained by using a Bruker D8 advanced instrument equipped with Cu-K α radiation (λ = 0.15406 nm). ZF-8 black-box ultraviolet lamp (6 W) was used as light source with reflective filter size is 200 × 80 mm. A TECH XT-5 melting point apparatus and LED lamp (25 W) were used as sources for thermal bleaching and visible light-induced photobleaching, respectively.

Preparation of compounds

The synthesis processes of the compounds are showed in Scheme 2. 1,3-Diphenyl-5-pyrazolone (DPP) was synthesized according to the method described in the literature.^{31,32}

1,3-Diphenyl-4-(3-chloro-4-pyridylformyl)-5-hydroxypyrazolone (DP3Cl4PyP) was synthesized with analogous method according to literature.³³ DP3Cl4PyP was directly used to the next reaction without further purify. Yield: 94%. Mp 82.2–84.1 °C. ¹H NMR (400 MHz, DMSO-*d*₆): δ = 11.354 (s, 1H, Pz-OH), 8.347 (d, J = 4.8 Hz,



Scheme 2 Synthesis of compound **1**, (a) PhNHNH₂, EtOH, 45 °C, 1 h; (b) 2-chloropyridine-4-carbonyl chloride, 1,4-dioxane, Ca(OH)₂, 80 °C, 2 h, HCl (3 M), r.t.; (c) PSC, EtOH, EtOAc, 80 °C, 3 h, r.t.

1H, pyridine-ring), 7.818 (d, J = 3.6 Hz, 2H, phenyl-ring), 7.548–7.243 (m, 10H, phenyl-ring).

1,3-Diphenyl-4-(3-chloro-4-pyridylformyl)-5-hydroxypyrazolone 4-phenylsemicarbazone (**1**) was prepared with similarly method.³⁴ The mixture of DP3Cl4PyP (2 mmol) and PSC (2 mmol) were dissolved in ethanol (8 mL) containing a few drops of glacial acetic acid was stirred and refluxed for 3 h at 80 °C. After cooling down to room temperature, white powders were separated from the solution by filtration, then washed three times with ethanol. Yield: 46%. Mp 205.0–206.2 °C. ¹H NMR (400 MHz, DMSO-*d*₆): δ = 12.018 (s, 1H, Pz-OH), 10.188 (s, 1H, N5-H), 9.264 (s, 1H, N4-H), 8.339 (d, J = 5.2 Hz, 2H, pyridine-ring), 7.937 (dd, J = 1.2, 8.8 Hz, 2H, phenyl-ring), 7.777 (s, 1H, pyridine-ring), 7.600–7.498 (m, 7H, phenyl-ring), 7.374–7.251 (m, 6H, phenyl-ring), 7.034 (t, J = 7.6 Hz, 1H, phenyl-ring). ¹³C NMR (120 MHz, DMSO-*d*₆): δ = 152.124, 150.978, 150.348, 148.762, 147.532, 139.002, 138.577, 137.415, 129.097, 128.862, 128.824, 128.596, 126.596, 126.418, 126.000. FT-IR (cm⁻¹): 3364, 3347 ν (N-H), 3249 ν (O-H), 1653 ν (C=O), 1598 ν (C=N), 1555, 1459 ν (phenyl-ring), 1509, 1395 ν (pyrazole-ring).

Preparation of TCCP materials

A stock solution (3 mL) containing pure DPA (0.25 mM) or compound **1**, or mixed solution of compound **1** (2.5 mM) with different mass ratio DPA (DPA: 0%, 5%, 10%, 15% and 20%) in ethanol was quickly injected into poor solvent of deionized water (6 mL) under ultrasound. Then, the mixture maintained for 10 h at 30 °C to get co-aggregates. The co-aggregates was separated from mixture by centrifugation and dried for 5 h at 50 °C *in vacuo*.^{35,36}

Results and discussion

Photochromic properties and mechanism of **1** in crystalline state

Photochromic properties in crystalline state. The novel compound **1** exhibits well dual-response and fatigue resistance



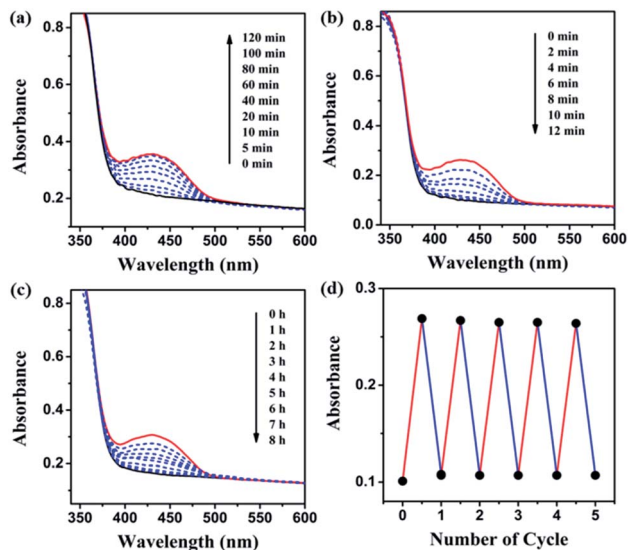


Fig. 1 Absorbance spectra under UV irradiation (a) and decolouring spectra of compound **1** (b) with visible light or (c) heating at 100 °C. (d) The colouration-bleaching cycles (red line: UV irradiation; blue line: heating or visible light).

performance in crystalline state. The absorption spectra of compound **1** were examined under UV light irradiation (365 nm) and varying visible light ($\lambda > 510$ nm) or heating at a temperature of 100 °C. Subsequently, a wide absorption band appeared and the absorption intensity around 380–500 nm continuously increased with the prolonged irradiation time (Fig. 1a). Meanwhile, the colour transformed from white to yellow. The colouring process obeys first-order kinetics with rate constant $2.26 \times 10^{-2} \text{ s}^{-1}$ for **1** (Fig. S4†). Fig. 1b and c illustrate that heating or visible light stimulation can decolour the photostationary state. The variations disclosed that **1** undergoes photochromic properties because of the photo-isomerisation from enol form (E-form) **1a** to keto form (K-form) **1b** in crystalline state. The fatigue resistance performance of compound **1** was characterized using UV-vis spectra specifying its high resistance to light and heat (Fig. 1d). Moreover, the fluorescence properties of compound **1** were further investigated in crystalline state. Fig. 2 illustrates the low fluorescent contrast of compound **1**.

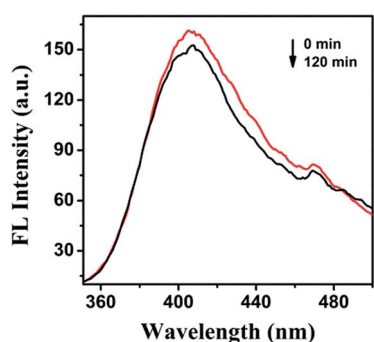
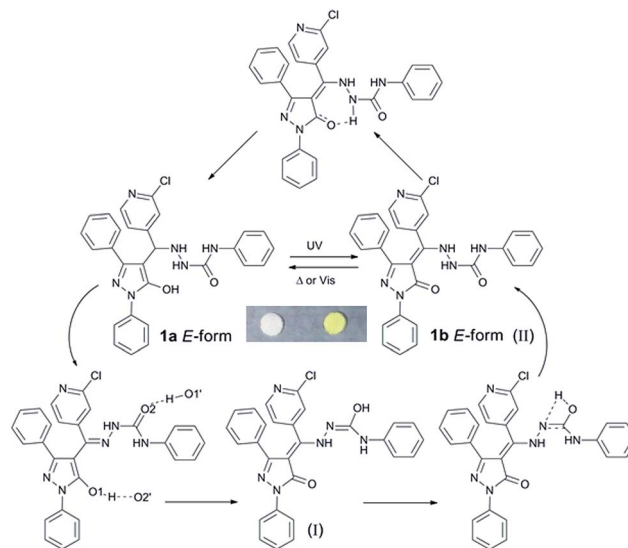


Fig. 2 Fluorescence spectra of **1** before irradiation (red line) and after irradiation (black line) with 365 nm light.



Scheme 3 Photochromic mechanism of compound **1** (': neighboring molecule).

Structure characterisation and photochromic mechanism

A detailed analysis of photochromic mechanism of compound **1** (Scheme 3) was conducted with IR, XPS spectra, crystal structure data and theoretical calculation as follows. The peak at 3249 cm^{-1} in IR spectra is assigned to O–H vibration, which shifted to lower wavenumber due to the strong hydrogen bonds within the crystalline state. Meanwhile, the apparent variation is ascribed to the isomerization of E-form and K-form (Fig. 3a). The crest of O–H vibration dissipates under the irradiation due to the formation of **1b**. With an ultimate objective to obtain the concrete tautomerism of **1**, the XPS spectrum was put into execution to distinguish the isomerization through binding energy changes of C–O and C=O. Therefore, O 1s spectra variation of **1** was monitored to verify the photochromic mechanism (Fig. 3b). The O 1s peak can be sectioned into two parts by curve fitting. The O 1s energy spectrum fitting peaks of E-form appear at 532.34 and 530.88 eV,³⁷ which can be assigned to C–O and C=O, and the integrated areas of energy spectrum peaks are 71% and 29%, correspondingly. Subsequently, the binding energies of K-form at 532.72 and 531.28 eV are ascribed to C–O and C=O, and the integrated areas are 51% and 49%,

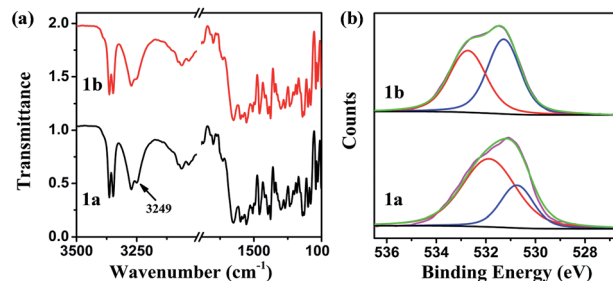


Fig. 3 (a) FT-IR spectra of **1** before UV irradiation (black) and after (red), (b) XPS spectra of O 1s before (**1a**) and after (**1b**) with 365 nm irradiation.



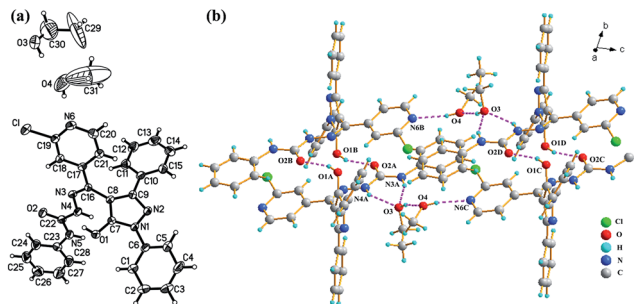


Fig. 4 (a) The crystal structure and (b) hydrogen-bonded connection diagram of compound 1.

respectively. The obvious variation can be implemented to estimate the photo-isomerization by related integrated areas. The integral areas of C=O increased but integral areas of C≡O decreased for colour-changed compound, reflecting the E-form **1a** is converted to K-form **1b**.

Single crystal X-ray diffraction was implemented to analysis the photochromic mechanism of pyrazolone derivative **1**. The single crystal of **1** was generated using slow evaporation of ethanol and methanol mixtures (1 : 2 v/v) at ambient temperature. The crystal data and structure refinement details were summarised in Table S1.† The corresponding bond length can be seen (Table S2†). The C7–O1 bond distance is 1.325(4), which is comparable to C–O single bond. The observations further prove that the sample of colourless **1** exist in E-form. Fig. 4a shows the crystal structure of compound **1**, where two solvent molecules are comprised in the unit of **1**. The dimer of compound **1** is formed by alternative intermolecular hydrogen bond [O(1)–H(10)···O(2)] as listed in Table S3,† and 1D chains are constructed through bridge hydrogen bond of solvent (Fig. 4b). Further, there exist no inherent hydrogen bonds between oxygen and nitrogen through the analysis of the hydrogen bonding in the single crystal structure. Therefore, it is valid to elaborate the photochromic mechanism of the tautomerization process of compound **1** *via* the multi-proton transfers. Firstly, the proton of the O1 atom is transferred to the O2 atom of the adjacent molecule and the proton of the O2 atom is transferred to the O1 atom of the neighboring molecule *via* the alternative intermolecular hydrogen bonds [O1–H···O2']. At the same time, the hydrogen of the N4 atom transfers to the N3 atom. And then, the hydrogen of O2 atom transfers to the N4 atom through the intramolecular hydrogen bond to form a K-form. In reverse reaction, hydrogen of the N4 atom was transferred to O1 atom with the intramolecular hydrogen bond to form E-form.

Quantum chemical calculation is a logical aspect to research the correlation between spectra and structure of molecules.^{38–40} Hence, we intended to obtain the colour-changed K-form under some spectroscopic parameters of UV-vis absorption through relationship spectra-structure to further confirm the rationality of photochromic mechanism. The six K-form isomers (I, II, III, IV, V, VI) were constructed on the premise of the E-form single crystal structure (Fig. S8†). All calculations in this report were carried out using the Gaussian 09 program.⁴¹ The structure of

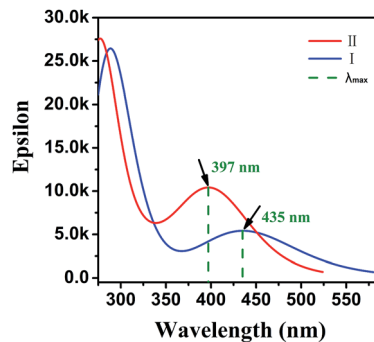


Fig. 5 The theoretical absorption spectra of K-form I and II with B3LYP/6-311G(d,p).

molecules were optimised and frequencies were calculated by implementing density functional theory (DFT) following the Becke3–Lee–Yang–Parr (B3LYP) with 6-31G(d,p) as basis set. UV-vis absorption along with HOMO and LUMO for six isomers at optimised geometry in the ground state were executed by employing TD-DFT approach with the B3LYP(54% HF) function assorted with the 6-311G(d,p) basis set in the gaseous phase, which were listed in Table S4.† The results illustrate that the K-form I, II and VI demonstrate peak absorptions at the visible region. Their absorption spectra are shown in Fig. S9† with Multiwfn analysis.⁴² Only the absorption spectrum profiles of isomers I and II was similar to experimental spectrum. TD-DFT calculation of I in the gaseous phase predicts three electronic transitions at 546, 453 and 403 nm with oscillator strength of 0.0070, 0.0964 and 0.0593 respectively. These absorptions are assigned to electron excitations of H → L (99%), H–1 → L (98%) and H–2 → L (94%) respectively. Two electronic transitions of II are 484 and 403 nm with oscillator strength 0.0088 and 0.2314 for electron excitations of H → L (99%), H–1 → L (98%). The maximum values of K-form I and II are at 435 nm and 397 nm, where, red-shifted by ~4 nm and blue-shifted by ~34 nm for experimental λ_{max} values coloured **1** (431 nm) respectively (Fig. 5). Although the maximum absorption of K-form I is close to the experiment result, the absorption ranges of II is more nearly experiment spectrum at visible area. This situation can be attributed to two aspects: (1) the excitation energy is directly dependent on the Hartree–Fock (HF) exchange percentage.^{43–46} (2) Colour-changed **1** may exist two K-forms of I and II. To this, the calculated relative sum of electronic and thermal free energies of II with respect to I is analysed. The relative value is about $-16.30 \text{ kcal mol}^{-1}$ (scale factor = 0.9614), which indicated that the isomerization reaction from I to II can be carry out spontaneously. The coloured K-form is confirmed according to theoretical calculations, which can further prove the rationality of our proposed photochromic mechanism.

The preparation and switchable properties of TCCM

The preparation and characterisation of TCCM. The TCCM were prepared with various contents of DPA by co-aggregating with 67% volume fractions of water left for aging with 10 h. The preparation details of optimisation condition were recorded in ESI.† Recipitates of DPA was also measured following



the time (Fig. S10†). Reprecipitates **DPA** take the shape of the schistose structure, and the width decrease with prolonging duration. However SEM spectra of different contents of **TCCM** barely possess schistose structure which also indicates that compound **1** can effectively control the morphology of **DPA** (Fig. 6a). In addition, the typical X-ray diffraction (XRD) of **TCCM** with smooth baseline shows significant differences (Fig. 6b). As the **DPA** content augments, the diffraction peak at $2\theta = 8.895$ degree gradually enhances and is consistent with patterns of **DPA**. However, characteristic diffraction peaks for compound **1** have almost no change at all. The results confirm that the crystalline of **TCCM** is basically stable.

The fluorescence switch properties of TCCM. The fluorescence spectra were performed to examine the switch properties of **TCCM**. Fluorescence intensity of the **TCCM** was collected at 445 nm before and after irradiation in crystalline state (Fig. 7a). The high fluorescence contrast can be reflected through the good fluorescence modulation rate. The fluorescence modulation ratio (FM ratio = $1 - I_{\text{off}}/I_{\text{on}}$)^{47,48} declined with **DPA** contents of 5% and 10%, while augmented with a further adding of **DPA** content. Besides, when the mole fraction of **DPA** in **TCCM** is as high as 10%, the switch exhibits an excellent fluorescence contrast of 79% in contrast to the crystalline-state **1** (FM ratio ~ 6%). Thus, 10% composites are regarded as an optimised molar ratio in this study. Fig. 7b shows the fluorescence regulation of 10% based on the irradiation time. The results showed that the energy donor of **DPA** could be effectively regulated with FRET using the photochromic reactions of energy acceptor **1** upon 365 nm light irradiation in crystalline state.

The FRET efficiency can be estimated using the fitting average lifetime according to eqn (1),^{49,50}

$$E_T = 1 - (\tau_1/\tau_2) \quad (1)$$

here, τ_1 and τ_2 are deemed as the fitting lifetime of **TCCM** before and after irradiation of 365 nm light irradiation in crystalline state. The energy transfer efficiency from the excited state of **DPA** to the K-form **1b** can be weighed using the fluorescence life analysis method. The fluorescence decay curves of reprecipitates **1** and **TCCM** are depicted at 445 nm before and after the irradiation at room temperature. The lifetimes of reprecipitates **1** exhibit no drastic variation before and after the irradiation, which indicates that the reprecipitates possess no substantial self-absorbance

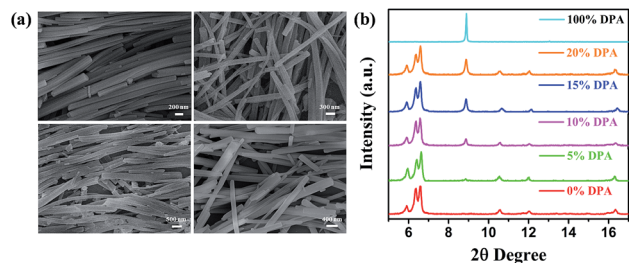


Fig. 6 (a) The SEM spectra of **TCCM** (A) 5%, (B) 10%, (C) 20%, (D) 30%, (b) powder XRD patterns of reprecipitates **1**, **DPA** and **TCCM** for aging 10 h.

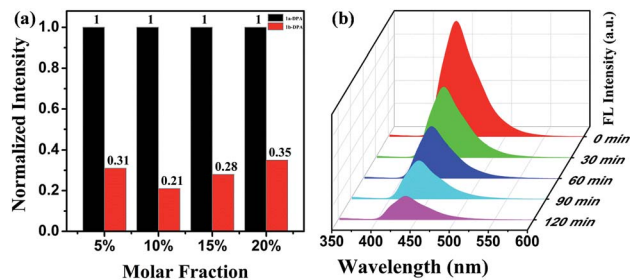


Fig. 7 (a) The normalized fluorescence intensities at 445 nm of **TCCM** in crystalline state before (black) and after (red) irradiation. (b) Fluorescence spectra changes of doping 10% **DPA** depending on the irradiation time, λ_{ex} : 350 nm.

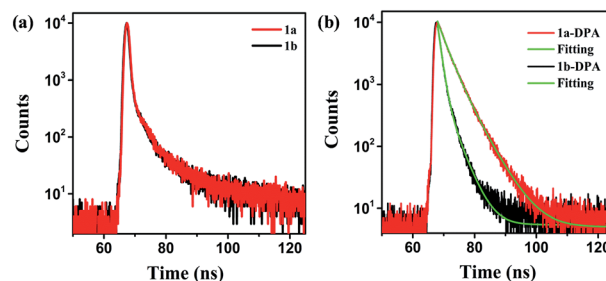


Fig. 8 (a) Fluorescence decay profiles of 10% before and after irradiation at room temperature. (b) Fluorescence decay curves of reprecipitates **1** before and after irradiation.

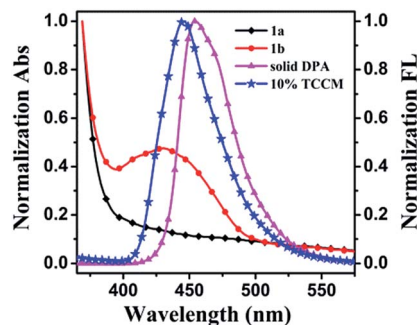


Fig. 9 The normalized overlay of emission spectra of **DPA** (purple line) and 10% **TCCM** (blue line) and absorption spectra of **1** before (black line) and after (red line) under irradiation with 365 nm light.

before and after irradiation (Fig. 8a). Whereas, the fluorescence decay curves of **TCCM** evidently exhibit the variations (Fig. 8b and S11†). The results elucidate that the FRET process takes place in **TCCM**. The energy transfer efficiency reaches to the maximum (55%) for 10% **TCCM** and the FRET tendency of **TCCM** is in contrast with FM ratio (Table S5†). The FM and FRET efficiency results indicate that the 10% **TCCM** is a more appropriate ratio. The impairment of fluorescence intensity can be closely associated with the well superimposed fluorescence spectra of fluorophore with the absorption spectra of K-form **1b** (Fig. 9), which should be beneficial for efficient FRET.^{51,52}



Conclusions

The novel dual-responded photochromic pyrazolone compound **1** with pyridine ring exhibits great photochromic properties and fatigue resistance ability in crystalline state. The fluorescence modulation of TCCM was realised through FRET from energy donor DPA to energy acceptor **1b** by photochromic reactions. The fluorescence contrast reaches to 79% with 55% energy transfer efficiency in optimised molar ratio of 10% TCCM. Based on his high-contrast fluorescent switch characteristic and inherent feature of photochromic material, TCCM may have potential application for data storage and switch.

Acknowledgements

This work is supported by the National Natural Science Foundation of China (21571152, 21262038 and U1203292), National 973 Program on Key Basic Research Project of China (2014CB660805), The Natural Science Foundation of Xinjiang Uygur Autonomous Region (2013211B04).

References

- G. Berkovic, V. Krongauz and V. Weiss, *Chem. Rev.*, 2000, **100**, 1741–1754.
- T. Fukaminato, *J. Photochem. Photobiol., C*, 2011, **12**, 177–208.
- H. Li and D. H. Qu, *Sci. China: Chem.*, 2015, **58**, 916–921.
- C. Yun, J. You, J. Kim, J. Huh and E. Kim, *J. Photochem. Photobiol., C*, 2009, **10**, 111–129.
- Y. Yokoyama, *Chem. Rev.*, 2000, **100**, 1717–1740.
- M. Irie, *Chem. Rev.*, 2000, **100**, 1685–1716.
- B. H. Rau, *Angew. Chem., Int. Ed. Engl.*, 1973, **12**, 224–235.
- M. Han and M. Hara, *J. Am. Chem. Soc.*, 2005, **127**, 10951–10955.
- F. M. Raymo and M. Tomasulo, *Chem. Soc. Rev.*, 2005, **34**, 327–336.
- G. Y. Jiang, S. Wang, W. F. Yuan, L. Jiang, Y. L. Song, H. Tian and D. B. Zhu, *Chem. Mater.*, 2006, **18**, 235–237.
- S. J. Lim, J. Seo and S. Y. Park, *J. Am. Chem. Soc.*, 2006, **128**, 14542–14547.
- S. Z. Pu, H. C. Ding, G. Liu, C. H. Zheng and H. Y. Xu, *J. Phys. Chem. C*, 2014, **118**, 7010–7017.
- A. J. Myles and N. R. Branda, *Adv. Funct. Mater.*, 2002, **12**, 167–173.
- J. Karnbratt, M. Hammarson, S. Li, H. L. Anderson, B. Albinsson and J. Andreasson, *Angew. Chem., Int. Ed.*, 2010, **49**, 1854–1857.
- M. Berberich, A. M. Krause, M. Orlandi, F. Scandola and F. Wurthner, *Angew. Chem., Int. Ed.*, 2008, **47**, 6616–6619.
- E. Deniz, S. Sortino and F. M. Raymo, *J. Phys. Chem. Lett.*, 2010, **1**, 1690–1693.
- A. Reisch, P. Didier, L. Richert, S. Oncul, Y. Arntz, Y. Mély and A. S. Klymchenko, *Nat. Commun.*, 2014, **5**, 4089.
- K. Trofymchuk, L. Prodi, A. Reisch, Y. Mély, K. Altenhöner, J. Mattay and A. S. Klymchenko, *J. Phys. Chem. Lett.*, 2015, **6**, 2259–2264.
- H. Li, J. X. Wang, H. Lin, L. Xu, W. Xu, R. M. Wang, Y. L. Song and D. B. Zhu, *Adv. Mater.*, 2010, **22**, 1237–1241.
- I. Yildiz, E. Deniz and F. M. Raymo, *Chem. Soc. Rev.*, 2009, **38**, 1859–1867.
- Y. Chen and N. Xie, *J. Mater. Chem.*, 2005, **15**, 3229–3232.
- M. Tomasulo, S. Giordani and F. M. Raymo, *Adv. Funct. Mater.*, 2005, **15**, 787–794.
- E. M. Lee, S. Y. Gwon, Y. A. Son and S. H. Kim, *J. Lumin.*, 2012, **132**, 1427–1431.
- J. X. Guo, L. Liu, G. F. Liu, D. Z. Jia and X. L. Xie, *Org. Lett.*, 2007, **9**, 3989–3992.
- J. X. Guo, D. Z. Jia, L. Liu, H. Yuan, M. X. Guo, D. L. Wu and F. Li, *J. Mater. Chem.*, 2011, **21**, 12202–12205.
- H. Yuan, J. Guo, D. Jia, M. Guo, L. Liu, D. Wu and F. Li, *Photochem. Photobiol. Sci.*, 2011, **10**, 1562–1567.
- J. X. Guo, Y. C. Zhang, D. Z. Jia, M. X. Guo and Y. H. Li, *Photochem. Photobiol. Sci.*, 2016, **15**, 1222–1226.
- L. Liu, H. B. Sun, S. Abdurehman, D. Z. Jia, J. X. Guo and D. L. Wu, *J. Photochem. Photobiol., A*, 2013, **267**, 55–59.
- Q. Liao, H. B. Fu and J. N. Yao, *Adv. Mater.*, 2009, **21**, 4153–4157.
- H. Tian and S. J. Yang, *Chem. Soc. Rev.*, 2004, **33**, 85–97.
- B. S. Jensen, *Acta Chem. Scand.*, 1959, **13**, 1668–1670.
- A. Akbarzadeh and R. Soleymani, *Orient. J. Chem.*, 2012, **28**, 153–164.
- J. X. Guo, D. Jia, L. Liu, H. Yuan and F. Li, *J. Mater. Chem.*, 2011, **21**, 3210–3235.
- H. Liu, J. X. Guo, D. Z. Jia, M. X. Guo, L. Liu and D. L. Wu, *New J. Chem.*, 2015, **39**, 9866–9871.
- Q. Liao, H. B. Fu, C. Wang and J. N. Yao, *Angew. Chem., Int. Ed.*, 2011, **50**, 4942–4946.
- H. Tong, Y. Dong, M. Häußler, J. W. Y. Lam, H. H. Y. Sung, I. D. Williams, J. Sun and B. Z. Tang, *Chem. Commun.*, 2006, **10**, 1133–1135.
- E. Ito, H. Oji, T. Araki, K. Oichi, H. Ishii, Y. Ouchi, T. Ohta, N. Kosugi, Y. Maruyama, Y. Naito, T. Inable and K. Seki, *J. Am. Chem. Soc.*, 1997, **119**, 6336–6344.
- S. A. Bhat and S. Ahmad, *J. Mol. Struct.*, 2016, **1105**, 169–177.
- M. Karabacak, M. Cinar, M. Kurt, A. Poiyamozi and N. Sundaraganesan, *Spectrochim. Acta, Part A*, 2014, **117**, 234–244.
- M. Karabacak, Z. Cinar, M. Kurt, S. Sudha and N. Sundaraganesan, *Spectrochim. Acta, Part A*, 2012, **85**, 179–189.
- M. J. Frisch, G. W. Trucks, H. B. Schlegel, *et al.*, *Gaussian 09 revision A.01*, Gaussian Inc, Wallingford, CT, 2010.
- T. Lu and F. Chen, *J. Comput. Chem.*, 2012, **33**, 580–592.
- M. Walker, A. J. A. Harvey, A. Sen and C. E. H. Dessent, *J. Phys. Chem. A*, 2013, **117**, 12590–12600.
- E. Vessally, S. S. Amiri, A. Hosseinian, L. Edjlali and A. Bekhradnia, *Phys. E*, 2016, **87**, 308–311.
- A. J. Cohen, P. Mori-Sánchez and W. Yang, *Chem. Rev.*, 2012, **112**, 289–320.
- J. Beheshtian, Z. Bagheri, M. Kamfiroozi and A. Ahmadi, *Microelectron. J.*, 2011, **42**, 1400–1403.
- M. Bossi, V. Belov, S. Polyakova and S. W. Hell, *Angew. Chem., Int. Ed.*, 2006, **45**, 7462–7465.



- 48 J. Folling, S. Polyakova, V. Belov, A. van Blaaderen, M. L. Bossi and S. W. Hell, *Small*, 2008, **4**, 134–142.
- 49 M. Tramier, I. Gautier, T. Piolot, S. Ravalet, K. Kemnitz, J. Coppey, C. Durieux, V. Mignotte and M. C. Moisan, *Biophys. J.*, 2002, **83**, 3570–3577.
- 50 A. Hoppe, K. Christensen and J. A. Swanson, *Biophys. J.*, 2002, **83**, 3652–3664.
- 51 B. K. An, S. K. Kwon, S. D. Jung and S. Y. Park, *J. Am. Chem. Soc.*, 2002, **124**, 14410–14415.
- 52 F. G. Shen, A. D. Peng, Y. Chen, Y. Dong, Z. W. Jiang, Y. B. Wang, H. B. Fu and J. N. Yao, *J. Phys. Chem. A*, 2008, **112**, 2206–2210.

